Proceedings of ASME Turbo Expo 2011
GT2011
June 6-10, 2011, Vancouver, British Columbia, Canada

GT2011-45204

PREDICTION OF TURBINE ROTOR BLADE FORCING DUE TO IN-SERVICE STATOR VANE TRAILING EDGE DAMAGE

Marcus Meyer, Roland Parchem, Peter Davison
Rolls-Royce Deutschland
Eschenweg 11, Dahlewitz
D-15827 Blankenfelde-Mahlow
Germany

ABSTRACT

In the following paper we will present an overview on the results of a research project whose objective is the assessment of the influence of trailing edge material loss of high pressure turbine nozzle guide vanes onto the low engine order excitation of the downstream rotor blade. To quantify the forcing, the modal forces for the rotor eigenmodes of interest are obtained by solving the unsteady Navier-Stokes equations for a full assembly of stator and rotor ring. Since the computing resources for such a calculation are too high to be routinely employed for the assessment of in-service damage patterns, an important task of the project was to investigate quick alternatives to the costly CFD simulations. The approach chosen is to perform a sufficient number of forced response calculations with different damage patterns in advance and use the results to build a surrogate model that can be used to assess the severity of damage patterns by simple interpolation. We will first present the analysis chain employed to quantify the forcing, next describe the approach to build a surrogate model with special focus on the generation of an optimal DoE matrix, and finally discuss the prediction accuracy of the surrogate model. It is shown that an interpolating surrogate model, based on radial basis functions, can successfully be used to predict the rotor forcing for damage patterns that were not analyzed using the costly CFD calculations beforehand.

INTRODUCTION

In this contribution we will give an overview on the results of a research project dedicated to the analysis of rotor forcing due to in-service damage. During the operation of jet engines it is possible that at the end of the nominal component life damage occurs at the trailing edges of the high pressure turbine nozzle guide vanes (HPT NGVs): Due to the extremely high temperatures in this region of the engine, which on average exceed the melting temperature of the employed vane material by more than 300 degrees during takeoff, any unintended decrease of the vane cooling mass flow can lead to a loss of trailing edge material, exemplary depicted in fig. 1. The structure of the NGV can withstand a significant amount of trailing edge material loss, thus the damage is posing no imminent threat to the operation of the engine.

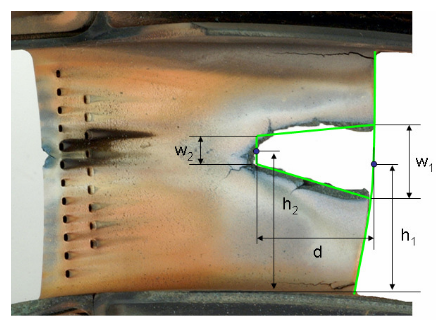

Fig. 1: Nozzle guide vane showing trailing edge material loss and the idealized shape parameterization

But additionally the damage changes the flow through the affected passage, thus causing a so-called low engine order excitation of the rotor bladerow downstream [1]. During normal operation of the engine a small amount of low order excitation is always present due to allowable tolerances in the static components, but the larger throat width variation caused by trailing edge material loss can lead –in extreme cases– to high cycle fatigue failure of a rotor blade, caused by a resonance in the operating range, which clearly has to be avoided at all cost. These resonances can be visualized in the so-called Campbell diagram, exemplary depicted in fig. 2 for an HPT rotor: In this example low engine orders (EO) in the interval from 7 to 12 intersect the frequency of the first rotor eigenmode in the operating range of the engine.

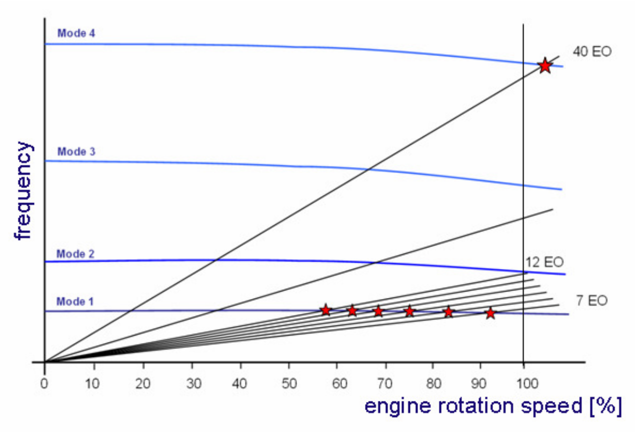

Fig. 2: Campbell diagram showing resonances for main and low engine order excitation

Thus it is very important to be able to accurately quantify the damage-induced rotor forcing if trailing edge damage is detected during routine engine inspections. Based on the shape (and circumferential distribution of the damage if more than one damaged vane is present), a maintenance schedule of the engine in question has to be assigned, which maximizes on-wing time without compromising the safe operation of the engine. Unfortunately both the individual shape of the damage as well as the circumferential distribution will be different from case to case. In addition it is necessary to solve the unsteady flow for a full NGV and rotor ring, typically modeled using the unsteady Reynolds-averaged Navier-Stokes equations (URANS) in order to accurately quantify the rotor forcing. Due to the large mesh that is required (approximately 40 million grid points) and the low frequency content that needs to be resolved, such a flow calculation can require up to 10 days on 40 cores on a high-performance cluster. This is clearly too time- and CPU-resource consuming for routine use. On the other hand a growing fleet of engines that enter service necessitate the capability of quick assessment of in-service damage patterns, defined by individual damage shapes and their circumferential distribution. Thus an important task of the research project at hand is to find an accurate prediction method with quick turnaround times. Our presentation is consequently structured into two parts: First we will describe the setup of the CFD simulation required for the quantification of rotor forcing and present steady and unsteady CFD results for a representative trailing edge damage. In the second part we will present the approach to build a surrogate model, investigate different surrogate formulations and assess the accuracy of the prediction results. The paper concludes with a summary and recommendations for future steps.

PART I - CFD ANALYSIS

The computations presented in this paper are performed using the Rolls-Royce proprietary code AU3D, an unsteady flow and aeroelasticity solver [2,3], which is based on unstructured meshes [5], thus offering high flexibility for modeling complex geometric shapes. The code solves the URANS equations with Spalart-Allmaras turbulence model and has been validated for a wide range of turbomachinery flows [4]. The structural part of the solver employs a modal model obtained from a 3D finite element representation of the rotor blade. The structural mode shapes (as example the first eigenmode of a typical HPT rotor blade is shown in fig. 3) are interpolated onto the fluid mesh in a preprocessing step. During the unsteady computation the structural and fluid boundary conditions, i.e. displacements and pressures, are exchanged at every time step. Although the solver permits movement of the fluid mesh to represent the instantaneous shape and position of the structure undergoing deformation under the influence of the fluid forces, the forced response calculations described in this paper are performed without mesh motion.

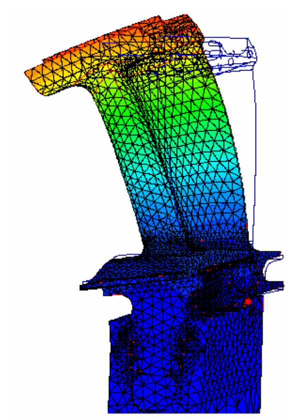

Fig. 3: First eigenmode of a typical HPT rotor blade

This decoupled approach, which is commonly employed for HPT rotor blades, reduces computing time and allows the computation of the forces acting on several eigenmodes and nodal diameters at once. (The nodal diameter denotes the number of vibration cycles around the circumference of the rotor ring.) This is important in our case because we do not know in advance which nodal diameter and eigenmode is excited the most by the damaged assembly under consideration. The modal forces obtained from the CFD solution are used in a subsequent step to calculate the rotor blade displacements and stresses, taking into account nonlinear elements such as under-platform dampers or seal wires, if present, using a frequency-domain nonlinear solver, see [12] and the references therein.

Grid generation

The assembly studied in this paper is representative of the first stage of modern high-pressure turbines. The geometry is taken from [13], where additional details on design and airfoil shapes can be found. Although the first two bladerows of high pressure turbines are normally cooled, the cooling flows were omitted in this study to allow comparison with the results of an upcoming measurement campaign, where cooling flows are also not present. The grids used for NGV and rotor blade row are hybrid meshes, consisting of 10 hexahedral element layers in the boundary layer and prismatic elements in the rest of the passage, see fig. 4. The meshes are unstructured in the blade-to-blade plane and the 3D grid is obtained by sweeping the unstructured mesh along the blade span [5]. The radial distribution of 100 grid layers and the parameterization of the unstructured mesh follows the recommendations of a mesh refinement study [7], undertaken to find reasonably sized meshes of high accuracy for this application. The resulting grid sizes of a single NGV and rotor blade passage are 400k points and 235k points, respectively, leading to a grid size of 32 million points for the full 2-row assembly, as shown in fig. 5 right.

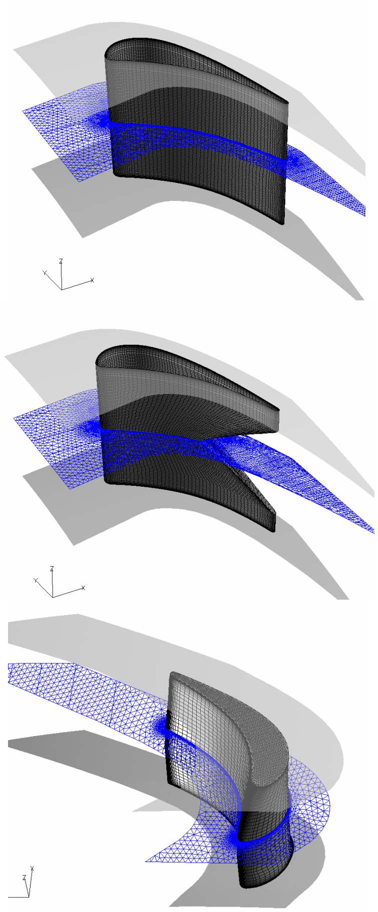

Fig. 4: Meshes used for datum vane (top), vane with triangular damage (middle) and rotor (bottom)

Fig. 5: Setup for steady (left) and unsteady (right) CFD calculations

Forced response calculation process

In the calculation process the first step consists in generating single passage NGV meshes for the specified individual damage shapes, and then assembling the individual passages to the full NGV ring. Additionally a single rotor passage with periodic boundary conditions is placed downstream of the NGV ring, as seen in fig. 5 left. This setup is solved until a steady flow state is reached, which yields the initial flow solution for the following time-accurate forced response calculation, where the full NGV ring is connected to the full ring of rotor blades, see fig. 5 right. For the calculation of the flow, prescribed radial distributions for total temperature, total pressure and flow angles are used as inflow boundary conditions, and a radial profile of static pressure is prescribed as exit boundary condition downstream of the rotor. The interface between the full NGV assembly and the single rotor passage is modeled as a mixing plane in the steady case and as a sliding plane in the unsteady case. The flow equations are advanced in time using second-order accurate implicit time integration with a constant time step that resolves the passing of one NGV pitch with 150 time steps. After each time step the current static pressure on the rotor blades is projected onto all specified eigenmodes and nodal diameters to yield the modal assembly forces. As can be seen from the Campbell diagram in fig. 2, low engine order resonances in this example can be expected to occur for the engine orders from 7 to 12. Ideally, a separate forced response calculation should be carried out to assess the resonance at the different speeds with the correct flow boundary conditions, but in order to reduce computational cost, the forced response analysis is only carried out for one representative speed, typically the takeoff speed. The levels of forcing are rescaled later to the appropriate resonance speeds of engine orders using the turbine inlet pressure, as described in [8].

Steady CFD analysis of a single damaged vane

In the following section we will present the results of the steady CFD analysis of a setup as depicted in fig. 5 (left). The NGV ring in this case includes one vane with a triangular damage, as shown in fig. 6. The large damage leads to the development of two strong vortices, which is shown in fig. 7, where the total pressure in the outlet plane of the NGV ring is depicted. It can be seen that the damage induces a window where the flow is turned significantly less than the flow in the undamaged vane passages, but the strong distortion is limited to a single passage left and right of the damaged vane. The wakes of the neighboring passages are affected only to a very small degree. This can also be clearly seen in fig. 8, where the Mach number on a radial cut at vane mid height is shown. Clearly the distortion is limited to the passages left and right of the damage. In addition we can see that the damage induces a region with an increased velocity on the suction side of the vane left to the damaged vane, which also leads to a reduction of the static pressure as seen in fig. 6. The influence of the distorted flow on the downstream rotor blade has to be assessed by an unsteady calculation, as presented in the next section.

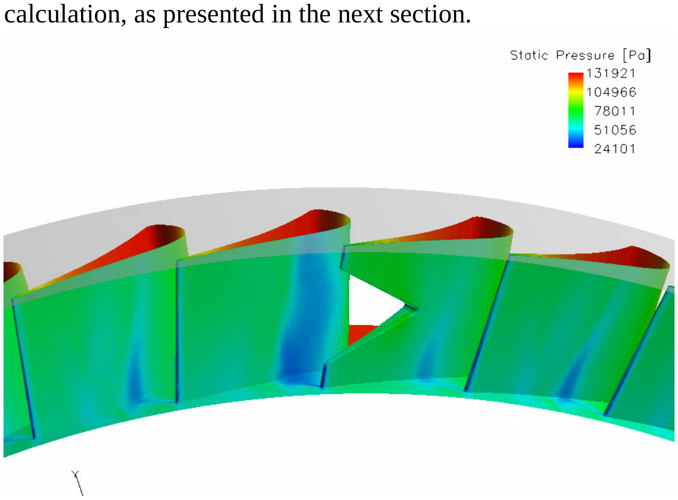

Fig. 6: Single triangular damaged vane surrounded by undamaged vanes

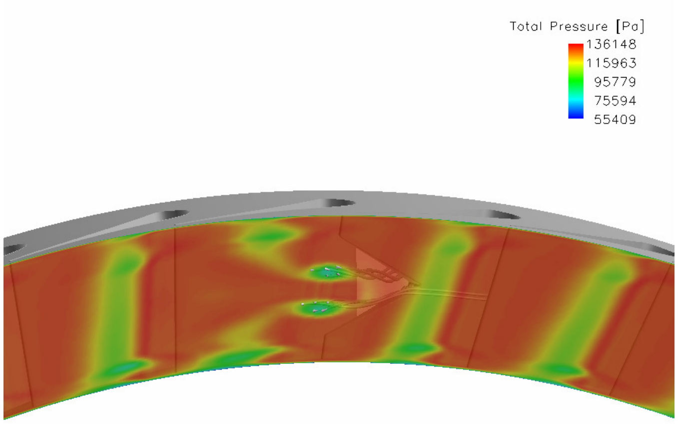

Fig. 7: Total pressure in the NGV exit plane behind a single triangular damage

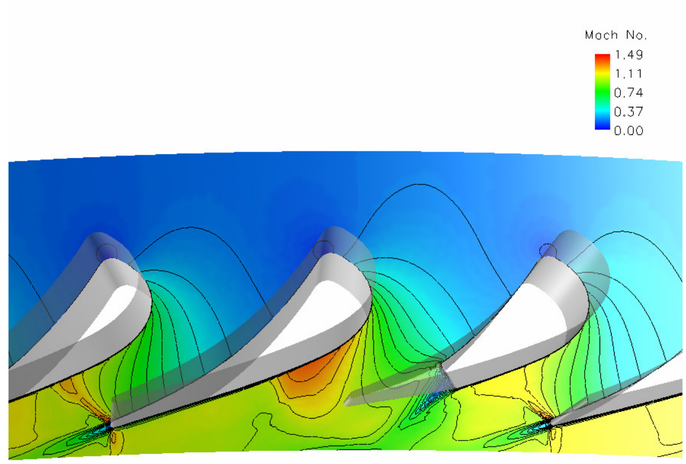

Fig. 8: Mach number on a radial cut at vane mid height

Unsteady results and low engine order excitation

In this section we will first describe the unsteady CFD results of the setup presented above, where a single vane with triangular damage is inserted into a ring with otherwise undamaged vanes, see fig. 9, where for clarification some of the rotor blades have been blanked, although the CFD setup includes the full rings of vane and rotor, as shown in fig. 5 right. As shown above in the analysis of the steady flow, the distortion is limited to the passage left and right of the damaged vane. The large window of flow with a significant under-turning compared to the non-distorted flow changes the loading of the rotor blade, as seen in fig. 10. Here the axial and tangential force per unit length on a radial cut at mid height of the rotor is compared for the undamaged case (dashed) and the passing of the damaged vane (full line), whose location is shown in fig. 9 together with lines indicating the corresponding time steps in fig. 10 below. It can be seen that the rotor first experiences an unloading in the tangential direction, followed by a stronger positive loading. This change of loading can excite the flap modes of the rotor blade, which we can assess by calculating the modal assembly force during the unsteady simulation, as described next.

To assess the modal forces for the low engine order excitation, the forced response analysis is carried out for 3500 time steps. This ensures that the modal force time history contains four cycles of the lowest (7th) engine order of interest, from which only the two last cycles will be used for the spectral analysis of the frequency content. As an example we will use the assembly depicted in fig. 11, where a large number of vanes with different damage sizes are placed randomly over the circumference. In fig. 12 the modal force of the 4th mode / 34th nodal diameter (ND) is compared for an undamaged and the randomly damaged assembly. Here mode 4/ND 34 corresponds to the main engine order excitation of the assembly. It can be seen that the amplitude of this excitation is lower for the damaged assembly, thus energy is redistributed to other frequencies, for example the mode 1/ND 7 excitation, which is shown in fig. 13. This excitation is not present at all in the undamaged assembly, but shows a significant modal force content for the damaged assembly. Which nodal diameter is excited the most depends on the frequency content of the flow and thus on the circumferential distribution of the damaged vanes. For the assembly depicted in fig. 12, the highest excitation is obtained for the 8th nodal diameter, as can be seen in fig. 14, where all low nodal diameter excitations of interest are compared.

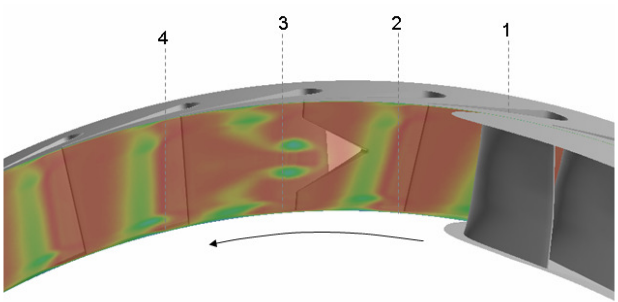

Fig. 9: Rotor passing a vane with triangular damage

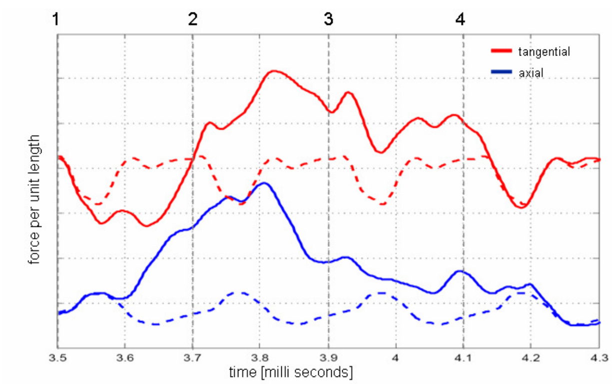

Fig. 10: Comparison of axial and radial rotor force per unit length at mid-height (dashed: undamaged, full: damaged assembly)

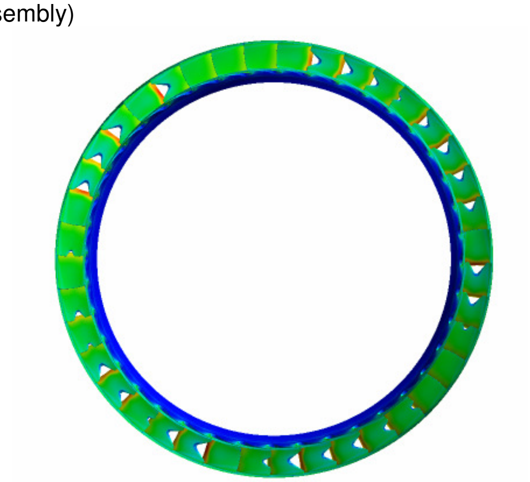

Fig. 11: NGV assembly with a large number of damaged vanes at random circumferential locations

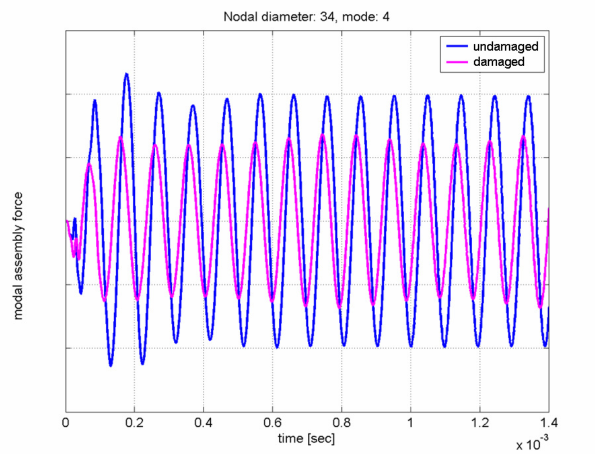

Fig. 12: Modal assembly force over time for mode 4 and nodal diameter 34 for undamaged (design 0) and randomly damaged case

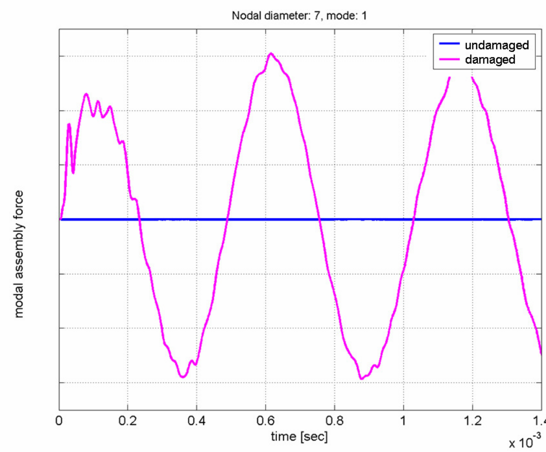

Fig. 13: Modal assembly force over time for mode 1 and nodal diameter 7 for undamaged and randomly damaged case

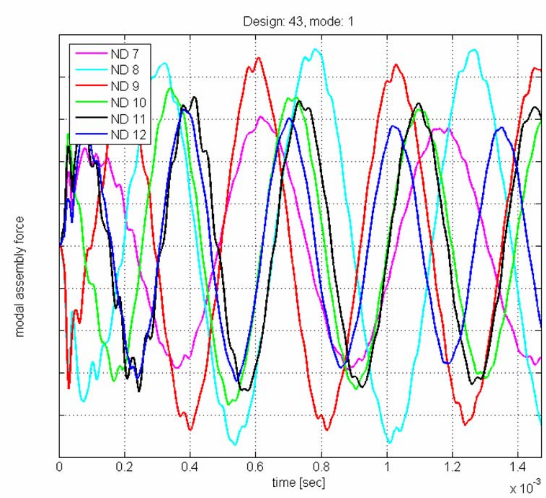

Fig. 14: Modal assembly forces for selected low nodal diameters over time for the randomly damaged case

PART II - SURROGATE MODELLING

An important task of the project is to develop an approach for a quick but accurate assessment method, which can deliver an answer in the order of minutes, i.e. does not require 10 days and an unsteady CFD analysis to quantify the rotor forcing. It was decided to employ an approach based on surrogate modeling techniques due to its general applicability. This approach requires a sufficiently high number of representative trailing edge damage shapes and their circumferential distributions to be simulated in advance using the CFD process described in the section above. Then a surrogate model is fitted to the CFD results and used for future predictions. In order for a surrogate based approach to be set up, we firstly need to define the input variables, secondly select an efficient Design-Of-Experiment (DoE) matrix, thirdly automate and run the process to perform the CFD calculation as well as its postprocessing, and finally decide on the functional form and fit the surrogate model to the data. These steps will be described in the following paragraphs.

Parameterization

The shape of the individual trailing edge material loss can for example be approximated with a trapezoid, as shown schematically in fig. 1. This parameterization requires five values to be specified for each damage, which has to be multiplied by the number of NGVs, typically of the order of 40, to arrive at the final dimension of the surrogate model space, in this case leading to a dimension of 40x5=200. This is clearly too high taking into account that a single forced response calculation requires 10 days on 40 cores, and at least 5 to 10 calculations should be performed per dimension. In order to reduce the dimensionality of the problem, an investigation of damage shapes which occur in service was carried out: Each of the available shape examples is approximated with a trapezoid. A subsequent statistical analysis of the resulting parameter values shows that fortunately (a) the damages mostly occur at midspan and (b) that the individual shape can be reconstructed from the area of the shape alone with a high degree of correlation. This means that if the area of the missing material is known, the shape which is most probable for this amount of missing area is given by an explicit functional relationship, shape = f(area). That greatly reduces the dimensionality of the problem to only a single free parameter per NGV. In addition it lowers the threshold for adoption of the proposed method in practice, since the effort to measure the size of missing trailing edge area is small, using for example an electronic borescope during routine in-service inspection.

The free parameters of our DoE setup are thus only the damage areas $\mathbf{a}$ of the individual NGVs. In addition we assign an upper bound to $\mathbf{a}$ based on experience. In order to limit the number of meshes of damaged NGVs that have to be generated for the DoE, a certain number of discrete levels $\mathbf{a}_i$ are selected, equally spaced between undamaged and maximal damage area. In our case i=6, leading to 7 different NGVs including the undamaged case, which form the building blocks of all damaged assemblies.

Generation of the DoE matrix

Before we proceed to generate the actual DoE matrix, we have to take into account the rotational symmetry of the CFD setup: It is common practice to ignore the circumferential variation of temperature, pressure and velocity, due to the integer number of burner cans spaced around the circumference. Instead a circumferentially averaged radial distribution of the combustor exit profile is specified. Thus the CFD assembly under consideration is rotationally symmetric with respect to the resulting forcing levels, even when trailing edge damages are present: Any duplicate of a damaged NGV ring that is created by rotating the whole NGV ring by an integer multiple of the pitch angle will yield the same forcing on the downstream rotor ring as the original non-rotated assembly. This fact fortunately reduces the required number of designs significantly, since each design point in the initial DoE matrix introduces all its rotated copies into the final "rotated" design matrix without the need to perform individual forced response calculations of these rotated copies. This will be exploited in the setup of the DoE matrix as follows: The matrix is built up from three parts: The first designs are selected to be single NGV damage cases of each discrete level $\mathbf{a}_i$, since those single damage cases are believed to occur most frequently during operation. The second set of designs are selected to be those cases that excite a pure engine order frequency in the engine operating range, i.e. the “worst case” scenarios. Those pure engine order excitation cases are created by placing 7 to 12 NGVs with maximal damage level as equally spaced as possible on the circumference of the NGV ring. The last set of 30 additional designs are chosen in such a way to evenly fill the design space (space-filling design). This can be achieved by using a simulated annealing optimization algorithm as described in [6]: Starting from an initial Latin hypercube design, the algorithm iteratively seeks to improve the space filling criterion, in our case the maximization of the minimal distance: A Latin hypercube design is called “maximin” when the separation distance $\min_{i \neq j} \|x_i - x_j\|$ is maximal among all Latin Hypercube designs of a given size. The distance is calculated for all possible combinations of (rotated) design sites. The algorithm selects “low-performing” designs which exhibit minimal distance and perturbs randomly selected entries of the corresponding design vectors to improve the space filling criterion. The minimal distances are evaluated also for all rotated copies of all designs in order to take the rotational symmetry into account and the algorithm is allowed to change only the last 30 designs in order to preserve the first two sets of the design matrix. The optimization is repeatedly started from different randomly generated initial Latin hypercube designs and the best solution found after several hundred optimization runs is selected as our final design matrix. If the rotational symmetry is taken into account, the resulting 43 designs represent a total of 1620 designs including the rotated copies, i.e. approximately 40 designs per degree of freedom. This number of points should be more than enough for the generation of an interpolating surrogate model with sufficient accuracy, as presented in the next section.

Surrogate model generation

Surrogate models, also called metamodels or response surfaces, can be subdivided into approximating and interpolating models. The approximating models are chosen when the output to be modeled contains random errors, for example when the results are obtained by performing measurements in the laboratory. In our case the results are obtained by performing computer experiments, and depend deterministically on the input parameters: If the same input parameters, i.e. damage areas for the NGVs in the assembly, are used for two forced response calculations, both will exhibit the same resulting modal force amplitudes. Thus in the case of computer experiments an interpolating model is the better choice [14]. For scattered data points in a high-dimensional space, the interpolating surrogate models which are most often employed are radial basis functions (RBF) [9], Kriging [10] and neural networks [11]. Since in our case the number of interpolations points (1620) and the dimension of the problem (40) are quite high, the optimization steps in both the Kriging and neural network approach can be very time consuming. Thus we will start with a radial basis function model and check the approximation quality using a cross validation technique. For the radial basis function model, the user has to specify the kind of basis function to use and the degree of the polynomial for the approximation of the global trend. In our case the functional form of the RBF model is given by

$$y(x) = \sum_{k=1}^{m} a_k \pi_k(x) + \sum_{j=1}^{M} b_j \varphi(x - x_j)$$

where the first term denotes the polynomial used to approximate the global trend and the second term the radial basis functions which describe the deviations of the model from the global function in order to obtain an interpolating model. The vector x denotes our free variables, i.e. the values of the missing area for each of the NGVs. Additional information on RBF models can be found in [9] and the references therein.

The correct choices for kernel φ and polynomial degree m are not obvious and differ from application to application. Thus we take a brute-force approach and fit RBF models for all possible combinations of basis function and polynomial degree, evaluate the goodness of fit by performing a cross validation for each model and finally select the model which displays the lowest error. The cross validation is performed by sequentially removing a single design from the full design matrix and rebuilding the RBF model with the reduced set of design points. Then the interpolated value for the removed design obtained from the RBF model is compared with the actual, known value, thus obtaining an error measure. The final root-mean-square (RMS) value of all relative error measures is used to select the best model for our application. The results of the cross validation are shown in fig. 15 for the 8th EO case and in fig. 16 for the 12th EO case. The kernel IDs correspond to the kernels {linear, cubic, thinplatespline, multiquadric, gaussian} and polynomial degrees {0,1}. These kernels are given by the functions

$$\varphi(z) = \begin{cases} \| z \| & (linear) \\ \| z \|^3 & (cubic) \\ \| z \|^2 \log(\| z \|) & (thinplatespline) \\ \sqrt{\| z \|^2 + \gamma^2} & (multiquadric) \\ \exp(\| z \|) & (Gaussian) \end{cases}$$

where z denotes the distance $\| x - x_j \|$. Since all RBF models with a polynomial degree 2 did exhibit a significantly higher error, they have been omitted from the figures 15 and 16.

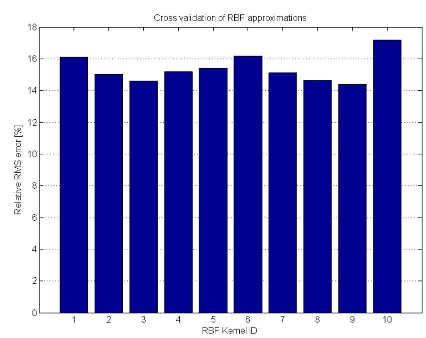

Fig. 15: Relative root mean square error for 8th EO content approximation with different radial basis function models

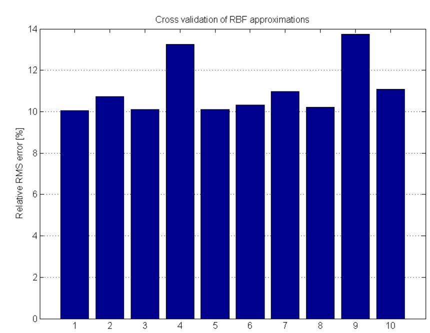

Fig. 16: Relative root mean square error for 12th EO content approximation with different radial basis function models

It can be seen that the influence of kernel and degree of polynomial on the RMS error is not very high, all models exhibit a relative error of around 15% for the 8th and 11% for the 12th EO case, which is surprisingly low given the very small number of only 43 CFD simulations that were performed. To improve the accuracy of the surrogate model, additional points can be added to the Design-of-Experiments matrix to improve the space-filling property. Another approach would be to switch to a Kriging surrogate model, which can be thought of as an optimized RBF model. In the Kriging model a typical kernel is given by the parameterized Gaussian kernel,

$$\varphi(z) = \exp(-\sum_{l=1}^{d} \theta_l \mid z_l \mid^{p_l})$$

where the free parameters θ_l can be thought of as "importance" factors, describing the influence of the individual input variable onto the surrogate response [15]. Since in our case, due to the rotational symmetry of the setup, it can be argued that each input variable is equally important, the optimization task to fit the Kriging model is simplified to a single-variable optimization, i.e. finding the $\theta_l = \theta$ which minimizes the Kriging MLSE error, or a two-variable optimization problem if also the exponent $p_l=p$ is allowed to vary. In order to assess the potential of improvement that can be gained by this optimization, a simple test is performed, where the RBF model with a Gaussian kernel is fitted for different values of theta in the range from 0.1 to 100 and the accuracy of the individual models is again estimated using the cross-validation approach. This test shows that the RMS error can be reduced by selecting the optimal theta value, but only by a small fraction of about 0.4%. Thus it can be concluded that the “tuned” RBF model with exponent p=2 and Gaussian Kernel is well suited for our application: In fig. 17 the model predictions for two different exponents (p=1 and p=2) are compared with the original data for a one-dimensional cut using the single-damage cases as reference. It can bee seen that the tuned RBF model with p=2 approximates the original data very well.

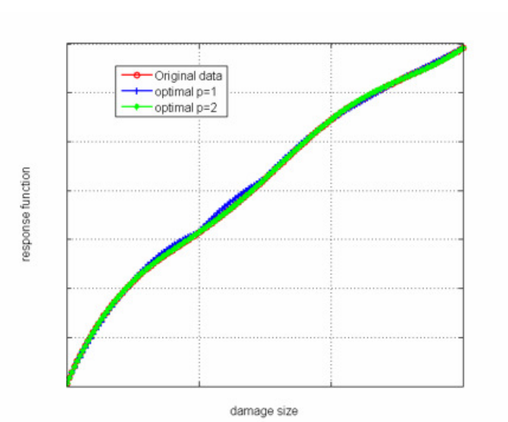

Fig. 17: Comparison of optimized Kriging model for exponents p=1 and p=2 with the original data (NGV ring with single damage of different size)

The resulting surrogate model can thus be used to predict the rotor forcing for assemblies that were not in the initial “training set”, i.e. the initial DoE matrix. The expected maximal error due to the interpolation model can be accounted for using a safety factor. In addition those designs that come up during service and are “far away” from the pre-computed designs can be analyzed with the unsteady CFD simulation. Then their forcing values are added to the surrogate model, thus creating a process of constant improvement of the surrogate model, based on the feedback from in-service inspections.

CONCLUSIONS AND OUTLOOK

In this paper the low engine order excitation of a high pressure turbine rotor blade due to NGVs with damaged trailing edges has been analyzed with the aim to generate a surrogate model for the quick assessment of damage severity. Due to the very high computing resources that are required for the analysis of low engine order excitation, the dimensionality of the design space has to be reduced as much as possible, which has been accomplished by a suitable parameterization of the damage shape, based on a statistical analysis. The process to generate a customized optimal design-of-experiment matrix that takes into account the rotational symmetry of the problem has been described. The generation of RBF surrogate models and its approximation quality has been presented. Future steps will aim at reducing this error by placing additional points at carefully selected design sites, based on in-service feedback. Additionally the sensitivity of modal force to the shape parameterization will be investigated to obtain an indicator of the error and possibly correction factors to account for the approximation of the individual damage shape by the simplified regression-based trapezoidal shape. Finally the results of an upcoming measurement campaign will be used to validate the CFD results, which will be described in a follow-up paper.

ACKNOLEDGEMENTS

The funding of this work under LUFO IV, Call I, Project RobusTurb, contract number 20T0608A is gratefully acknowledged. In addition the authors want to thank Dr. di Mare, Imperial College, London, for many helpful discussions, and Rolls-Royce Deutschland for allowing the publication of this work.

REFERENCES

[1] Breard, C., Green, J. H., Imregun,M.: Low-engine-order excitation mechanisms in axial-flow turbomachinery, Journal of Propulsion and Power, Vol. 19, No. 4, pp. 704-712, 2003.

[2] Sayma, A. I., Vahdati, M., Sbardella, L., Imregun, M.: Modeling of three-dimensional viscous compressible turbomachinery flows using unstructured hybrid grids. AIAA Journal, Vol. 38, No. 6, pp. 945-954, 2000

[3]Vahdati, M., Sayma, A.I., Imregun, M.: An integrated nonlinear approach for turbomachinery forced response prediction. Part I: Formulation. Fluids and Structures, Vol. 14, No. 1, pp. 87-101, 2000.

[4]Vahdati, M., Sayma, A.I., Imregun, M.: An integrated nonlinear approach for turbomachinery forced response prediction. Part II: Case studies. Fluids and Structures, Vol. 14, No. 1, pp. 103-125, 2000.

[5] Sbardella, L., Sayma, A.I., Imregun, M.: Semi-structured meshes for axial turbomachinery blades. International Journal for Numerical Methods in Fluids, Vol. 32, No. 5, pp. 569-584, 2000

[6] Husslage, B., Rennen, G., van Dam, E., den Hertog, D.: "Space-Filling Latin Hypercube Designs for Computer Experiments" (March 2006). Available at SSRN: http://ssrn.com/abstract=895464

[7] Popig, F.: Numerische Analyse der Strömung in einer Statorpassage mit beschädigter Hinterkante. Studienarbeit, Technische Universität Cottbus, 2008

[8] Green, J.S., Fransson, T.: Scaling of Turbine Blade Unsteady Pressures For Rapid Forced Response Assessment, GT2006-90613, Proceedings of the ASME TurboExpo, 2006

[9] M. J. D. Powell: Radial basis functions for multivariable interpolation: A review, In: Algorithms for approximation, Clarendon Press, 1987, pp 143 – 167

[10] Stein, M. L.: Interpolation of Spatial Data: Some Theory for Kriging, Springer Series in Statistics, 1999

[11] Poggio, T. Girosi, F.: Networks for approximation and learning, Proceedings of the IEEE, Vol. 78, No. 9, 1990, pp. 1481-1497

[12] Petrov, E. P., Ewins, D.J.: Advanced modelling of underplatform friction dampers for analysis of bladed disc vibration, ASME: Journal of Turbomachinery, 2007, Vol.129, January, pp.143-150

[13] AdTurb Synthesis Report ADTB-RR-0011, http://www.energy.kth.se/ADTURB2/documents/reports/ADTurB-synthesis.pdf

[14] Sacks et al: Design and Analyis of Computer Experiments, Statist. Sci., Vol. 4, No. 4 (1989), pp. 409--423

[15] Forrester, A., Sobester, A., Keane, A.: Engineering Design via Surrogate Modelling: A Practical Guide, John Wiley & Sons, 2008

